

# Excitons and stacking order in h-BN

Romain Bourrellier,<sup>1</sup> Michele Amato,<sup>1,2</sup> Luiz Henrique Galvão Tizei,<sup>1</sup> Christine Giorgetti,<sup>2</sup> Alexandre Gloter,<sup>1</sup> Malcolm I. Heggie,<sup>3</sup> Katia March,<sup>1</sup> Odile Stéphan,<sup>1</sup> Lucia Reining,<sup>2</sup> Mathieu Kociak,<sup>1</sup> and Alberto Zobelli<sup>1,\*</sup>

<sup>1</sup>*Laboratoire de Physique des Solides, Univ. Paris-Sud, CNRS UMR 8502, F-91405, Orsay, France*

<sup>2</sup>*Laboratoire des Solides Irradiés, Ecole Polytechnique, Route de Saclay,*

*F-91128 Palaiseau and European Theoretical Spectroscopy Facility (ETSF), France*

<sup>3</sup>*Department of Chemistry, University of Surrey, Guildford GU2 7XH, United Kingdom*

The strong excitonic emission at 5.75 eV of hexagonal boron nitride (h-BN) makes this material one of the most promising candidate for light emitting devices in the far ultraviolet (UV). However, single excitons occur only in perfect monocrystals that are extremely hard to synthesize, while regular h-BN samples present a complex emission spectrum with several additional peaks. The microscopic origin of these additional emissions has not yet been understood. In this work we address this problem using an experimental and theoretical approach that combines nanometric resolved cathodoluminescence, high resolution transmission electron microscopy and state of the art theoretical spectroscopy methods. We demonstrate that emission spectra are strongly inhomogeneous within individual flakes and that additional excitons occur at structural deformations, such as faceted plane folds, that lead to local changes of the h-BN stacking order.

In the last years, hexagonal boron nitride (h-BN) emerged as a promising alternative candidate for optoelectronic applications in the far UV region [1, 2]. An efficient BN based ultraviolet (UV) light emitter in the 5.3-5.9 eV energy range has been recently obtained using accelerated electrons as the pumping source [3]. For the design of future h-BN devices it is fundamental to have an in-depth description and understanding of the complex luminescence of this material.

Theoretical and experimental works have demonstrated that the emission spectrum of h-BN is dominated by a Frenkel type exciton at 5.75 eV [1, 2]. However, a single peak emission appears only in high quality macroscopic crystals that can be obtained only in a limited amount through high pressure and high temperature synthesis processes [4]. Common h-BN samples present a more complex emission spectrum with a series of sharp emissions close to the main exciton in the 5.3-5.9 eV energy range. An additional broad emission occurs within the electronic band gap in the energy range 3.2-4.5 eV on which a series of three sharp lines might be superposed depending on the BN sample purity [4, 5].

The origin of this complex emission pattern is still controversial and it has been attributed to the presence of unidentified structural defects. Impurities have been proposed to be responsible for emission lines in the band gap [4] and generic dislocations or grain boundaries to be at the origin of emission lines near the free exciton. The latter hypothesis has been suggested by the appearance of additional emission peaks when a pristine perfect crystal was deformed by a limited mechanical strain [7, 8]. Furthermore, it has been shown through sub-micrometric emission maps obtained by cathodoluminescence (CL) filtered images that the standard exciton is homogeneous in a h-BN crystallite whereas additional peaks present some spatial localization [9, 10]. However, research conducted in the last ten years has not yet been able to correlate

the optical properties of h-BN with the microscopic structure of defects. Here we address this fundamental question by adopting a theoretical and experimental approach combining few nanometer resolved cathodoluminescence techniques [11] with high resolution transmission electron microscopy images and state of the art quantum mechanical simulations. We show how additional excitonic emissions are associated with changes in the layer stacking order and how these structures can appear at local layers folds.

h-BN flakes with an average lateral size of about 2-3  $\mu\text{m}$  and thickness from a few nanometers down to the monolayer were obtained by chemical exfoliation through ultrasonication in isopropanol of commercially available micrometric powder. Luminescence within individual h-BN nanoflakes was investigated at a nanometric resolution through cathodoluminescence hyperspectral imaging. Individual particles were scanned by a 1 nm electron probe in a scanning transmission electron microscope (STEM) and a full emission spectrum in the 3.0-6.0 eV energy range was acquired at each probe position together with a bright field and a high angle annular dark field image, HAADF (a full emission spectrum is shown in supplementary figure 1). In this work we will focus on excitonic emissions in the 5.3-5.9 eV energy range, the most interesting spectral region for optical applications [3], leaving to future discussion additional emissions appearing occasionally in the middle of the band gap.

In figure 4.a,b we present bright field and HAADF images synchronously acquired with a hyperspectral image ( $9 \cdot 10^4$  sequential spectra obtained while scanning the sample). A series of five emission lines at 5.30, 5.46, 5.62, 5.75 and 5.86 eV is clearly visible in the overall cathodoluminescence spectrum of the nanoparticle (Fig. 4.c). These energies correspond to previously reported values for h-BN crystals and multi-walled BN nanotubes [10, 12]. Photoluminescence experiments conducted at

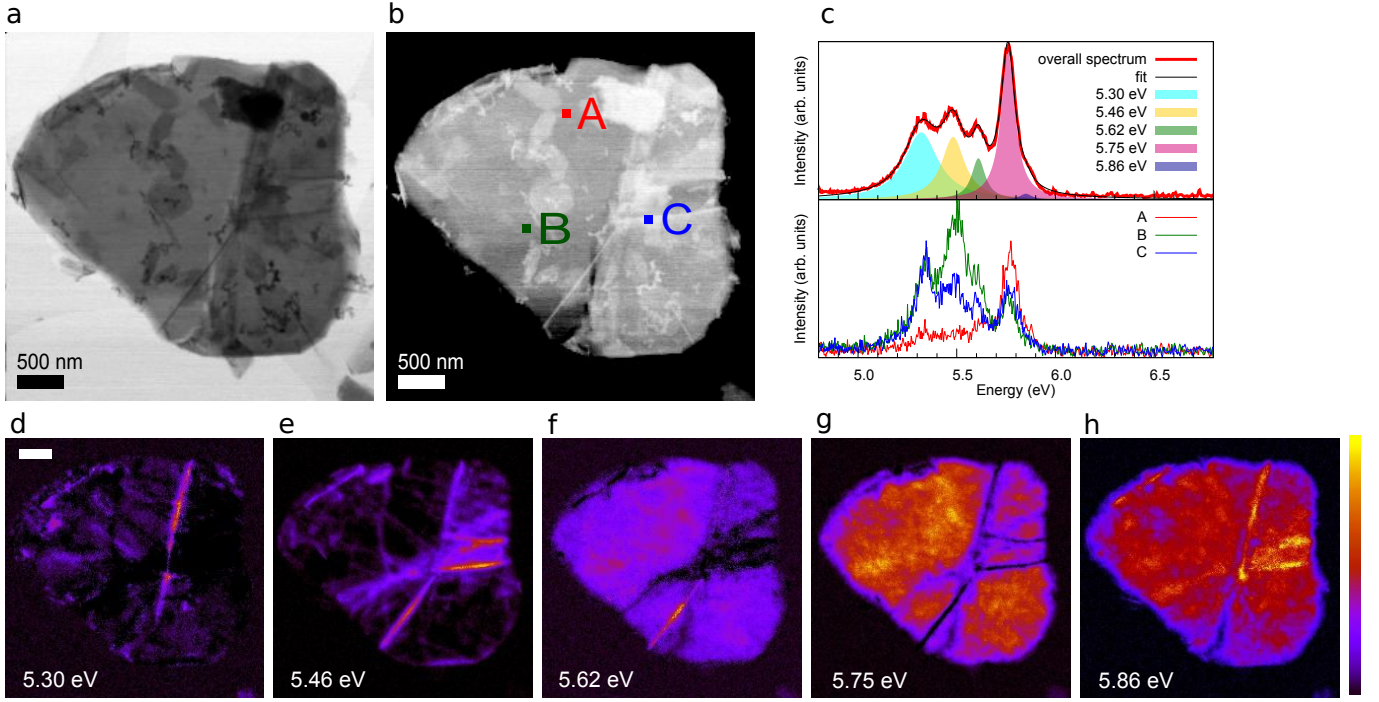


Figure 1. **a** Bright field and **b** dark field images of an individual BN flake. **c** Overall emission spectrum of the flake and individual spectra taken at specific probe positions indicated in panel **b**. **d-h** Emission maps for individual emission peak. Intensity is normalized independently within each individual map.

different temperatures show finer structures for temperatures below 50 K [12]. These additional features are smeared at higher temperature and thus are not visible through our experimental set up operating at about 150 K.

The three example spectra presented in Fig. 4.c show the strong inhomogeneities in the peak's relative intensities occurring at different probe positions. Thin samples present regions in which only the h-BN bulk exciton, usually called the free exciton, occurs (supplementary figure 2). In order to extract the spectral weight of individual emission lines, a multi-Lorentzian fitting routine has been applied to each spectrum of the spectrum image. Whereas peak energies were free parameters of the fitting procedure, no relevant energy shifts were detected across individual and between different flakes. Intensity maps derived from this analysis are shown in figure 4.d-h. Each map has been normalized independently on the basis of the most intense pixel. It should be mentioned however that peaks at 5.62 and 5.86 eV are systematically significantly weaker than other emission lines and this behavior can not be attributed solely to detection efficiency differences.

A detailed analysis of intensity maps demonstrates strong inhomogeneities occurring at lines crossing the flakes. The free excitonic emission at 5.75 eV and the two emission peaks at 5.62 eV and 5.86 eV are distributed all across the particle. Contrarily, the two emission peaks at

5.30 eV and 5.46 eV are mostly localized at the lines. All emission maps are clearly not correlated one with another and thus all five emission features should be considered independent.

Lines visible in CL maps appear also clearly in HAADF and bright field images and thus they are associated with local structural changes. Furthermore they occur mostly in pairs separated by few up to hundred of nanometers (supplementary figure 3). For a better understanding on how specific emission peaks are associated with specific structural features, these lines have been characterized by bright field imaging in an aberration corrected STEM.

In figure 2.g we present a HAADF image for a pair of parallel bright lines and the corresponding scanning transmission bright field focal series (Fig. 2.a-f). Each line is formed by two parallel fringes indicating layers parallel to the electron beam direction. The under-focused image (Fig. 2.a) is rather similar to the image of a double walled BN nanotube, but unlike the case of a nanotube the focus for the two series of fringes occurs at two different defocus values (Fig. 2.b,c). This corresponds to a situation where the two series of fringes lie at different depths. Finally when both pairs of fringes are overfocused the image of the underlying h-BN lattice is recovered (Fig. 2.e,f). A similar behavior is found also for structures with a higher number of fringes (supplementary figure 4).

The behavior described here can be explained by a model in which a layer stack can deform forming two

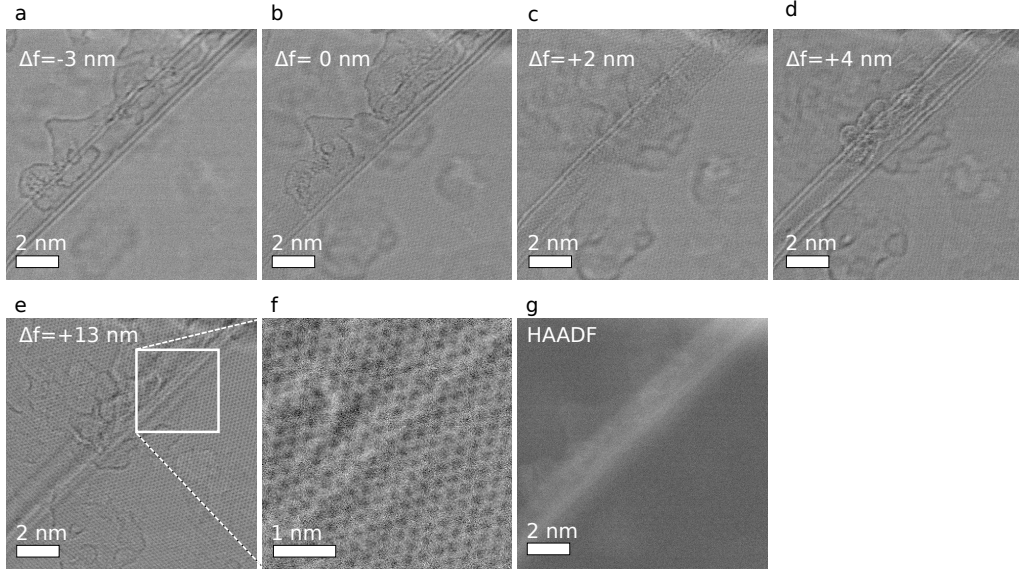


Figure 2. **a-e**. Five micrographs of two couple of parallel fringes extracted from a 34-image focal series. The two pair of fringes are focussed at different focal depths **f** Magnified image showing that the fringes are aligned along an arm-chair direction of the h-BN lattice. **g**. Dark field image of the region showing a local increase of the projected density at the fold.

almost parallel folds (see Fig. 3). This double folded structure has been proposed to occur in neutron irradiated graphite [13] and it has been recently imaged in CVD grown few-layer graphene [5, 6] and MoS<sub>2</sub> flakes [16]. Our observations do not allow to exclude the additional presence of single folds whereas they might be less common than double folds. Emission peaks at energies of 5.30 eV and 5.46 eV are thus solely associated with folds.

The different curvature of the layers at the fold induces, as for any multi layered structure, a relative glide of the layers and thus a loss of the original AA' stacking sequence of the perfect h-BN crystal (Fig. 3). The local atomic structure of the folds is thus analogous to the structure of multi walled nanotubes where in principle no defined stacking sequence exists. However, in multi-walled BN nanotubes and in other inorganic nanotubes the competition between bending and interplane energies tends to localize the curvature and to promote polygonal tube sections with facets of well defined stacking, not necessarily AA' [17–19]. The local atomic structure at the fold's facets should thus correspond to stacking sequences that can be generated from the original AA' structure by a glide of the layers. Two metastable configurations can then be obtained by translating one of the basal planes by a vector  $t \cdot (1/3, 2/3, 0)$ , with  $t$  a real number. For  $t = 1$  the AB<sub>1</sub> structure is obtained, where, following an analogous nomenclature for graphite nitrogen and boron atoms lies at  $\alpha$  and  $\beta$  sites respectively, and for  $t = 2$ , the AB<sub>2</sub> structure, where atoms positions are inverted (Fig. 3) [20–22]. If the fold follows an armchair direction, as is seen most often in scanning transmission bright

field images (Fig. 2.f,g), antiphase domains appear in the region between the folds. The stacking of planes at antiphase domain boundaries corresponds to a metastable AA order or, by applying an additional translation, an AB<sub>3</sub> order (Fig. 3). Besides the specific fold case, antiphase domains are, as for graphite, a common defect in h-BN and indeed AA stacking orders have been recently identified in few layer h-BN crystals [23].

These topological considerations suggest that additional excitonic peaks should be associated solely with changes of the crystal symmetry in the above-mentioned five possible stacking sequences. In order to confirm this hypothesis we have performed a complementary theoretical investigation of the optical spectra for these configurations. It has been successfully demonstrated that fundamental insights on emission can be provided by an analysis of simulated absorption spectra, taking into account that absolute energies could not be accessed due to the neglect of Stokes shifts [2, 12, 24]. Wave functions were obtained in the framework of density functional theory using the local density approximation and quasi particle energies were corrected by a subsequent GW treatment [25]. In a first step, optical spectra were evaluated in the random phase approximation (RPA). Finally, electron hole interactions, associated with excitonic effects that dominate the h-BN optical spectra, have been included by solving the Bethe-Salpeter equation (BSE) [26]. This computational scheme has been successfully applied to the study of the absorption spectrum of h-BN and BN nanotubes [2, 24, 27, 28]. Due to the well known underestimation of the h-BN band gap in the non self consistent GW computational scheme a 0.35 eV rigid shift has been

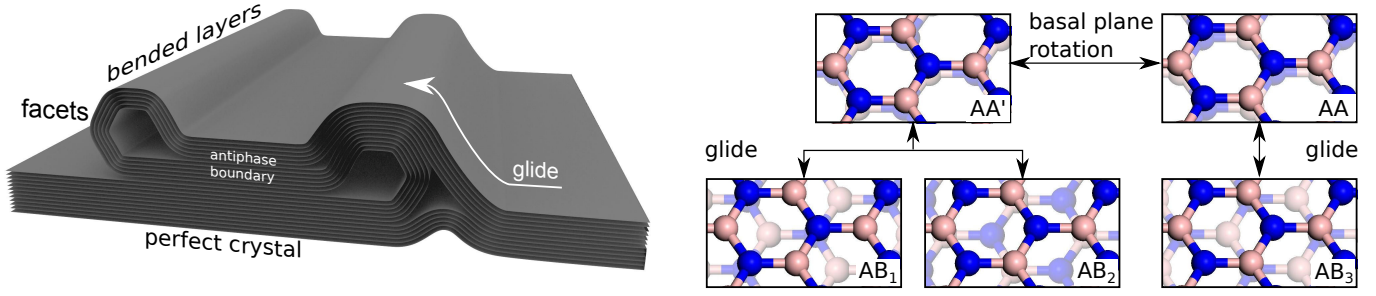


Figure 3. **Left.** Model of a faceted double fold in a h-BN crystal. At different sections of the crystal layers glides and antiphase boundaries appear. **Right.** Morphological deformations promote transition to different stacking sequences. Layers glide at bended regions transforms the original AA' stacking in the AB<sub>1</sub> or AB<sub>2</sub> stackings. AA and AB<sub>3</sub> are associated to antiphase boundaries in overlapping regions.

applied to all spectra that allows the alignment of the excitonic peak of the AA' stacking to the known experimental value.

For different h-BN polytypes, bands dispersion remains invariant in the  $a^* b^*$  plane. However for directions parallel to the  $c^*$  axis the last two occupied and first two unoccupied bands are either degenerate or split depending on stacking order. This leads to changes in the direct band gap observed both at the DFT and GW level (see Table 1 in the supplementary materials). This behavior has also a fundamental role in defining the optical properties of different stacking configurations. Indeed in agreement with the work of Arnaud et al. on AA' h-BN [29], we find for all configurations that directions parallel to the  $c^*$  axis give rise to the first absorption peak of  $\epsilon_2$  both at RPA and BSE levels. Quasi-particle band gaps and exciton binding energies are finally strongly dependent on the stacking order and determine the energies of optically active excitons (more details will be provided in a future work).

All absorption spectra presented in Fig. 4 show strong excitons with well separated energies in the range between 5.2 to 5.9 eV depending on the stacking configuration. Taking as a reference the standard AA' exciton

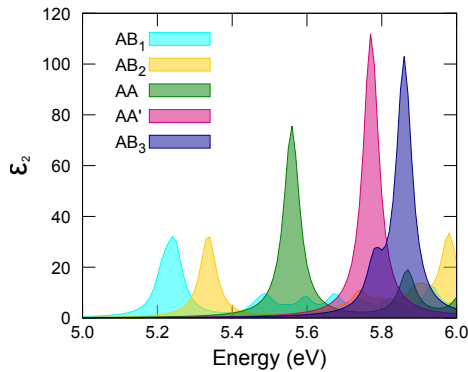


Figure 4. Imaginary part of the dielectric function (optical absorption spectrum) for different h-BN stacking obtained in the framework of GW+BSE calculations.

at 5.75 eV, three additional excitons, associated with the AB<sub>1</sub>, AB<sub>2</sub> and AA configurations, occur at lower energies whereas that of the AB<sub>3</sub> configuration is found at a higher one. Energy range and peak distribution coincide with experimental results. Thus theoretical simulations enable us to associate each of the five measured emission peaks with the five high symmetry configurations analyzed. In particular emissions at 5.30 and 5.46 eV, strongly localized at folds, can be attributed to AB<sub>1</sub> and AB<sub>2</sub> stacking sequences respectively. These models are compatible with the faceted fold structure where discrete layer glides between facets give rise to well defined stacking orders. Emissions at 5.62 and 5.86 eV can be associated with the AA and AB<sub>3</sub> stacking respectively. Since these stackings appear at antiphase boundaries, these excitons occur in large regions of the flake and their signal is weak due to the small number of atomic planes involved. We underline that each intermediate stacking gives rise to different exciton energies (supplementary figure 5). The experimental evidence for only five discrete emission lines is thus a clear indication of a finite number of stacking configurations and it confirms the hypothesis of faceted folds.

In conclusion, using a complementary experimental and theoretical approach we have provided a microscopic explanation for the complex emission spectrum of h-BN relating local changes in the layer stacking order to the appearance of additional excitons. Furthermore, we have shown how these defects and the associated excitonic emissions can be strongly localized at folds crossing the flakes. Finally our theoretical analysis reveals that, whereas additional emission lines in h-BN can still be interpreted as excitons bound to defects, they can be better described as bulk excitons of different polytypes. Recently, h-BN polytypes have been discussed from a morphological and energetic point of view but little attention was paid to their optical and electronic properties [20–23]. This study emphasizes the role of stacking changes in defining the optical properties of h-BN. The importance of stacking faults is thus directly related to



the interest in h-BN as one of the most promising materials for high performance far ultraviolet emitters.

The authors acknowledge support from the Agence Nationale de la Recherche (ANR), program of future investment TEMPOS- CHROMATEM (No. ANR-10-EQPX- 50), and Triangle de la Physique, Theo-STEM project (No. 2010-085T). The work has also received funding from the European Union in Seventh Framework Programme (No. FP7/2007- 2013) under Grant Agreement No. n312483 (ESTEEM2) and Marie Curie Intra-European Fellowship No. 326794 (EXPRESS).

---

\* alberto.zobelli@u-psud.fr

- [1] K. Watanabe, T. Taniguchi, and H. Kanda, *Nat. Mater.* **3**, 404 (2004).
- [2] L. Wirtz, A. Marini, M. Gruning, and A. Rubio, *arXiv:cond-mat/0508421* (2005).
- [3] K. Watanabe, T. Taniguchi, T. Niiyama, K. Miya, and M. Taniguchi, *Nat. Photon.* **3**, 591 (2009).
- [4] Y. Kubota, K. Watanabe, O. Tsuda, and T. Taniguchi, *Science* **317**, 932 (2007).
- [5] L. Museur, D. Anglos, J.-P. Petitot, J.-P. Michel, and A. V. Kanaev, *J. Lumin.* **127**, 595 (2007).
- [4] L. Museur, E. Feldbach, and A. Kanaev, *Phys. Rev. B* **78**, 155204 (2008).
- [7] K. Watanabe, T. Taniguchi, T. Kuroda, and H. Kanda, *Diamond Relat. Mater.* **15**, 1891 (2006).
- [8] K. Watanabe, T. Taniguchi, T. Kuroda, and H. Kanda, *Appl. Phys. Lett.* **89**, 141902 (2006).
- [9] P. Jaffrennou, J. Barjon, J. S. Lauret, B. Attal-Trétout, F. Ducastelle, and A. Loiseau, *J. Appl. Phys.* **102**, 116102 (2007).
- [10] P. Jaffrennou, J. Barjon, T. Schmid, L. Museur, A. Kanaev, J.-S. Lauret, C. Y. Zhi, C. Tang, Y. Bando, D. Golberg, B. Attal-Trétout, F. Ducastelle, and A. Loiseau, *Phys. Rev. B* **77**, 235422 (2008).
- [11] L. F. Zagonel, S. Mazzucco, M. Tence, K. March, R. Bernard, B. Laslier, G. Jacopin, M. Tchernycheva, L. Rigutti, F. H. Julien, R. Songmuang, and M. Kociak, *Nano Lett.* **11**, 568 (2010).
- [12] K. Watanabe and T. Taniguchi, *Physical Review B* **79**, 193104 (2009).
- [13] M. I. Heggie, I. Suarez-Martinez, C. Davidson, and G. Haffenden, *J. Nucl. Mater.* **413**, 150 (2011).
- [5] A. W. Robertson, A. Bachmatiuk, Y. A. Wu, F. Schäffel, B. Büchner, M. H. Rummeli, and J. H. Warner, *ACS Nano* **5**, 9984 (2011).
- [6] K. Kim, Z. Lee, B. D. Malone, K. T. Chan, B. Alemán, W. Regan, W. Gannett, M. F. Crommie, M. L. Cohen, and A. Zettl, *Phys. Rev. B* **83**, 245433 (2011).
- [16] A. Castellanos-Gomez, R. Roldán, E. Cappelluti, M. Buscema, F. Guinea, H. S. J. Van der Zant, and G. A. Steele, *Nano Lett.* (2013), 10.1021/nl402875m.
- [17] A. Celik-Aktas, J.-M. Zuo, J. F. Stubbins, C. Tang, and Y. Bando, *Acta Cryst. A* **61**, 533 (2005).
- [18] K. Tibbetts, R. Doe, and G. Ceder, *Phys. Rev. B* **80**, 014102 (2009).
- [19] D. Golberg, M. Mitome, Y. Bando, C. Tang, and C. Zhi, *Appl. Phys. A* **88**, 347 (2007).
- [20] N. Marom, J. Bernstein, J. Garel, A. Tkatchenko, E. Joselevich, L. Kronik, and O. Hod, *Phys. Rev. Lett.* **105**, 046801 (2010).
- [21] J. Yin, M. Hu, Z. Yu, C. Zhang, L. Sun, and J. Zhong, *Physica B* **406**, 2293 (2011).
- [22] G. Constantinescu, A. Kuc, and T. Heine, *Phys. Rev. Lett.* **111**, 036104 (2013).
- [23] A. Shmeliov, J. S. Kim, K. B. Borisenko, P. Wang, E. Okunishi, M. Shannon, A. I. Kirkland, P. D. Nellist, and V. Nicolosi, *Nanoscale* **5**, 2290 (2013).
- [24] L. Wirtz, A. Marini, M. Gruning, C. Attacalite, G. Kresse, and A. Rubio, *Phys. Rev. Lett.* **100**, 189701 (2008).
- [25] L. Hedin, *Phys. Rev.* **139**, A796 (1965).
- [26] G. Onida, L. Reining, and A. Rubio, *Rev. Mod. Phys.* **74**, 601 (2002).
- [27] C. Attacalite, M. Bockstedte, A. Marini, A. Rubio, and L. Wirtz, *Phys. Rev. B* **83**, 144115 (2011).
- [28] S. Galambosi, L. Wirtz, J. A. Soininen, J. Serrano, A. Marini, K. Watanabe, T. Taniguchi, S. Huotari, A. Rubio, and K. Hämäläinen, *Phys. Rev. B* **83**, 081413 (2011).
- [29] B. Arnaud, S. Lebgue, P. Rabiller, and M. Alouani, *Phys. Rev. Lett.* **96**, 026402 (2006).

## Supplementary informations

### SYNTHESIS

Few-layer hexagonal boron nitride flakes was obtained by chemical exfoliation following the protocol presented in Ref [1]. A solution of 10 mg of h-BN powder in 10 ml of isopropanol was sonicated for 7 hours and subsequently centrifuged for 120 minutes at 500 revolutions per minute. The supernatant was then dropped onto a TEM copper grid. Samples were then purified by a three hour 500 °C thermal treatment in a 800 mbar forming gas atmosphere (95% N<sub>2</sub>, 5% H<sub>2</sub>). HREM images and core level electron energy loss spectroscopy confirmed the absence of any carbon contamination due to solvent residuals. Flakes presented a lateral size of few microns.

### MICROSCOPY AND SPECTROSCOPY

Cathodoluminescence was performed in a dedicated VG-HB501 scanning transmission electron microscope operating at 60 keV, below the atomic displacement threshold for h-BN in order to avoid irradiation damage [2, 3]. Optical spectra were collected using an optical spectrometer with a 300 groove diffraction grating blazed at 300 nm. The resolution of the CCD was 0.17 nm/pixel.

High resolution scanning transmission electron microscopy images were recorded in a NION ULTRA-STEM 200 microscope operating at 60 keV. Lattice

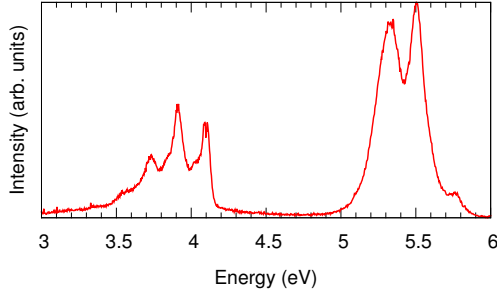


Figure 1. Full emission spectrum recorded for an h-BN flake on which additional intraband emission appears.

planes were visible in bright field images but not in dark field due to the resolution loss at low voltage and the rather high thickness and orientation complexity of the sample.

### Cathodoluminescence

In figure 1 is shown a full emission spectrum of a h-BN flake in the energy range from 3 to 6 eV. Besides high energy emission peaks commented in the main article, an additional intraband broad emission appears in the energy range 3.2-4.5 eV on which three sharp peaks at 3.73, 3.90 and 4.09 eV are superposed. These additional emission features occur occasionally in limited regions of the flakes. Previous photoluminescence studies have attributed the broad emission to donor acceptor pairs and the sharp lines to phonon replicas of a luminescent impurity [4]. The spatial localization of these signals obtained through cathodoluminescence will be discussed in a future work.

In figure 2 we present cathodoluminescence maps obtained for a thin h-BN flake. Spectra extracted from the original hyperspectral image show that single emission lines can appear in different regions of the flake. In the spectrum C it is solely visible the 5.75 eV emission line characteristic of a perfect h-BN crystal. This indicates that thin regions can be defect free and have the standard AA' stacking of h-BN.

### Microscopy images

Figure 3 shows low magnification scanning transmission electron microscopy (STEM) high angle annular dark field images (HAADF) of three h-BN flakes where two bright lines separated by few hundred nanometers are visible. The structure is similar to previous observations of double folds in few-layer CVD grown graphene [5, 6]. As discussed by Robertson et al. [5] folds can be parallel (as in figure 3.a) or form a narrow angle depending on

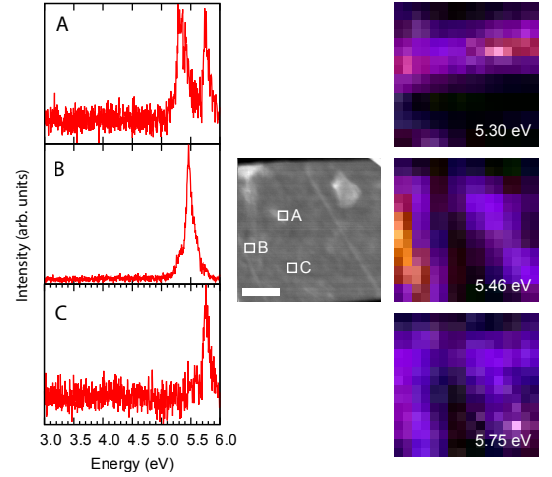


Figure 2. **Left.** Spectra extracted from a cathodoluminescence hyperspectral image for probe position indicated in the **middle** HAADF image. **Right.** Cathodoluminescence emission maps of the 5.30, 5.46 and 5.75 eV emission peaks.

the fold's directions with respect to the graphene lattice. In figure 3.c a local increase of the projected density in the region between the two lines is visible. This local thickening of the flake is compatible with the double fold model proposed in this work (see figure 3 of the article).

In figure 4 we present (Fig. 4.a) a low magnification HAADF image of a bright line and (Fig. 4.b-e) emission maps of four excitonic peaks extracted from a hyperspectral cathodoluminescence image. As discussed in the article, peaks at 5.30 and 5.46 eV are strongly localized at the folds. At a higher magnification the bright line appears as being formed by two parallel lines separated by about 10 nm (Fig. 4.f). The same region has been imaged through a high resolution bright field focal series obtained in an aberration corrected scanning transmission electron microscope (Fig. 4.g-l). Each line of the dark field image is constituted of five parallel fringes indicating layers parallel to the electron beam direction. The focus for the two series of fringes occurs at two different defocus values. The structure can thus be interpreted as a double fold involving five h-BN planes.

### THEORY

Quantum mechanical calculations of electronic and optical properties for the five stacking configurations of bulk h-BN were performed following a well established computational procedure. Ground state electronic structures were derived using plane waves pseudo-potential density functional theory as implemented in the Abinit package within the local density approximation (LDA). A Monkhorst-pack grid of  $10 \times 10 \times 4$   $k$ -point was used to sample the Brillouin zone of the system. An energy cutoff of 32 Ha was demonstrated to be enough for the

convergence of the total energy. Following the ground state calculations, self energy corrections to the Kohn-Sham eigenvalues for high symmetry points of the Brillouin zone was obtained using many body perturbation theory (MBPT) adopting a non self-consistent GW approach. The  $6 \times 6 \times 2$   $k$ -grid for GW calculations was not shifted meaning that the Gamma point was included. Since for all the structures the dispersion of the GW correction was lower than 0.5 eV, a scissor operator, chosen at the Gamma point, has been used for the optical spectra calculation.

In a first step, optical spectra were evaluated in the random phase approximation (RPA). Dielectric functions were derived using a  $15 \times 15 \times 7$  shifted  $k$ -grid and 30 energy bands. Crystal local field effects were included (with 50 G vectors) and a scissor operator was applied to take into account GW self energy corrections. In a second step, we performed optical spectra calculations by using the Bethe-Salpeter equation, which permits to include electron-hole interaction by mixing all the electronic transitions in the resolution of a two particle equation. A  $15 \times 15 \times 7$  shifted  $k$ -grid was used, with 50 G-vectors and a broadening of 0.025 eV.

In table I we report LDA direct band gaps, quasi particle corrections at the gamma point (scissor operator applied), optical gap and energy of the first optical active exciton for the five h-BN polytypes considered. Both band gaps and exciton binding energies contribute to the determination of the energy of the first optical active exciton.

The two metastable configurations AB<sub>1</sub> and AB<sub>2</sub> can be obtained from the AA' structure by translating one of the basal planes by a vector  $t \cdot (1/3, 2/3, 0)$  where  $t$  assumes the value 1 and 2 respectively (Fig. 5). In order to

investigate the effect on the optical properties of a continuum variation between high symmetry configurations to model the glide, absorption spectra have been computed following a GW+BSE scheme for three additional configurations with  $t=0.25, 0.5$  and  $0.75$ . In Fig. 5 it is shown that a different absorption spectrum is associated with each configuration. The experimental observation of only five excitonic emission peaks is thus a clear indication for a limited number of high symmetry stacking configurations present in the crystals.

---

\* alberto.zobelli@u-psud.fr

- [1] J. N. Coleman, M. Lotya, A. O'Neill, S. D. Bergin, P. J. King, U. Khan, K. Young, A. Gaucher, S. De, R. J. Smith, I. V. Shvets, S. K. Arora, G. Stanton, H.-Y. Kim, K. Lee, G. T. Kim, G. S. Duesberg, T. Hallam, J. J. Boland, J. J. Wang, J. F. Donegan, J. C. Grunlan, G. Moriarty, A. Shmeliov, R. J. Nicholls, J. M. Perkins, E. M. Grievson, K. Theuwissen, D. W. McComb, P. D. Nellist, and V. Nicolosi, *Science* **331**, 568 (2011).
- [2] A. Zobelli, A. Gloter, C. P. Ewels, G. Seifert, and C. Colliex, *Phys. Rev. B* **75**, 245402 (2007).
- [3] J. Kotakoski, C. H. Jin, O. Lehtinen, K. Suenaga, and A. V. Krasheninnikov, *Phys. Rev. B* **82**, 113404 (2010).
- [4] L. Museur, E. Feldbach, and A. Kanaev, *Phys. Rev. B* **78**, 155204 (2008).
- [5] A. W. Robertson, A. Bachmatiuk, Y. A. Wu, F. Schäffel, B. Büchner, M. H. Rummeli, and J. H. Warner, *ACS Nano* **5**, 9984 (2011).
- [6] K. Kim, Z. Lee, B. D. Malone, K. T. Chan, B. Alemán, W. Regan, W. Gannett, M. F. Crommie, M. L. Cohen, and A. Zettl, *Phys. Rev. B* **83**, 245433 (2011).

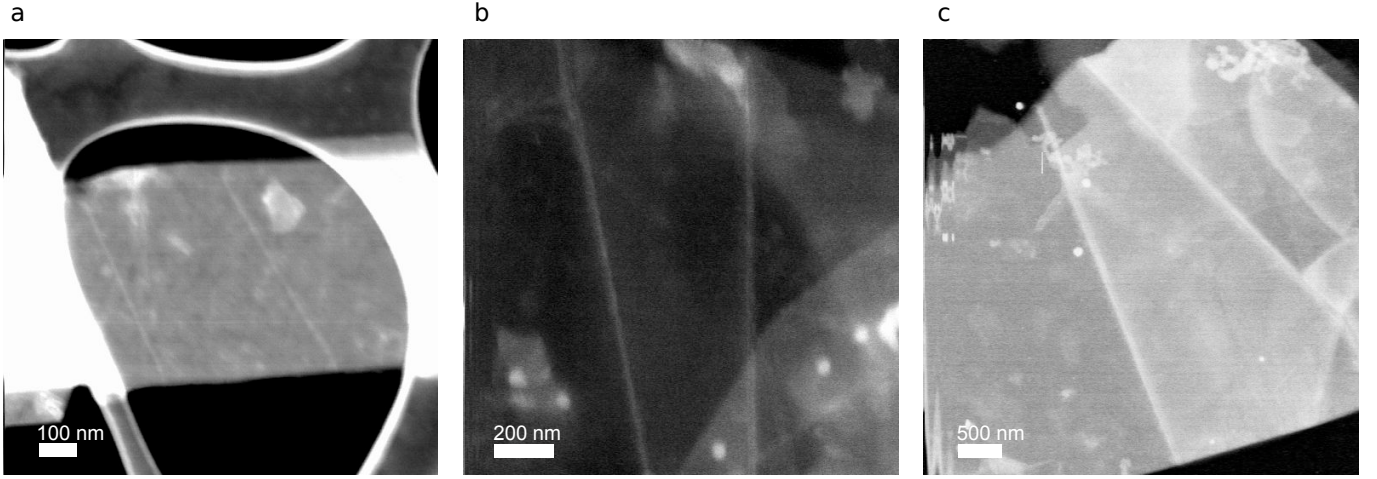


Figure 3. Low magnification HAADF images for different h-BN flakes where a series of almost parallel bright lines appear.

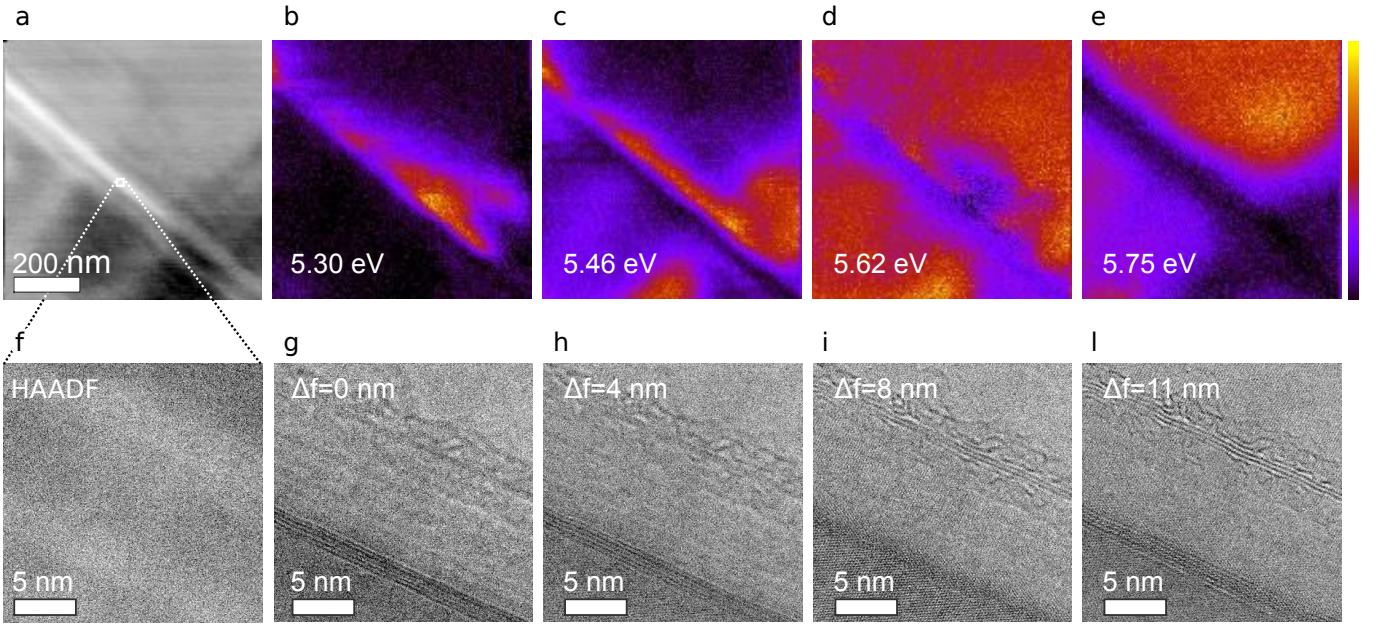


Figure 4. **a.** Low magnification HAADF image of a line in a h-BN flake and **b-e** cathodoluminescence maps of the region corresponding to different excitons. **f.** Higher magnification HAADF image of the same zone and four bright field micrographs extracted from a 40 image focal series.

Configuration	LDA direct gap	GW correction at the $\Gamma$ point	RPA optical gap	First optical active exciton transition energy	Exciton binding energy
AB <sub>1</sub>	3.51	1.72	5.23	4.89	0.34
AB <sub>2</sub>	3.70	1.75	5.45	4.98	0.47
AA	2.95	1.72	5.70	5.21	0.49
AA'	4.52	1.67	6.19	5.42	0.77
AB <sub>3</sub>	4.35	1.74	6.09	5.43	0.66

Table I. DFT-LDA direct gap, GW correction at the  $\Gamma$  point, RPA optical gap, BSE first optical active exciton energy and exciton binding energy calculated for different h-BN stacking configurations. All energies are expressed in eV.



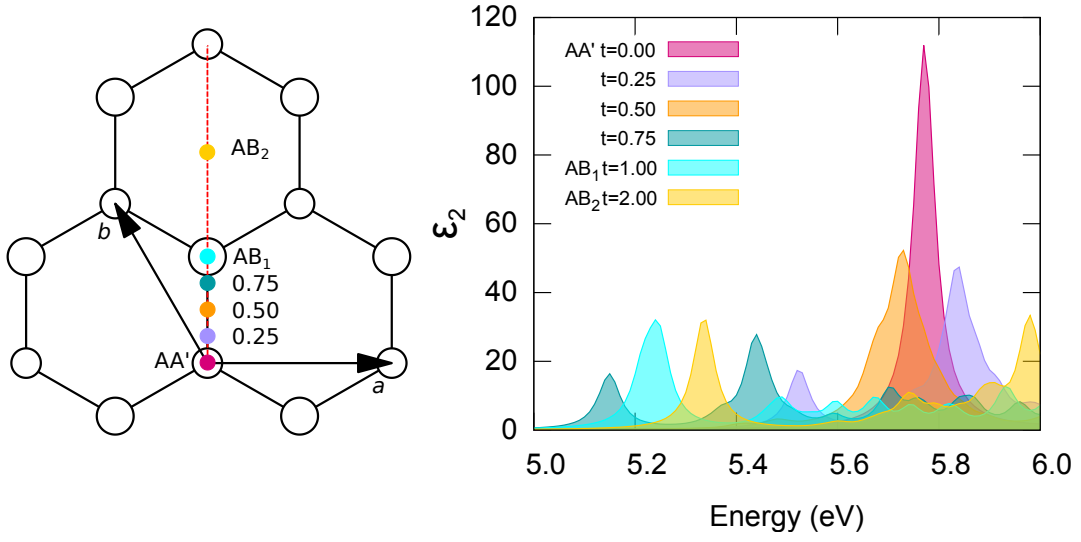


Figure 5. **Left** Schematic representation of the transformation of AA' h-BN in the AB<sub>1</sub>, AB<sub>2</sub> and intermediate stacking configurations obtained by gliding one basal plane by a vector  $t \cdot (1/3, 2/3, 0)$ . **Right** Imaginary part of the dielectric function (optical absorption spectrum) for different h-BN stacking derived in the framework of GW+BSE calculations.